Molecular Dynamics Simulations of Methane Hydrate Using Polarizable Force Fields

ARTICLE *in* THE JOURNAL OF PHYSICAL CHEMISTRY B · JULY 2007

Impact Factor: 3.3 · DOI: 10.1021/jp068505k · Source: PubMed

3 AUTHORS, INCLUDING:

Hao Jiang

22 PUBLICATIONS **397** CITATIONS

SEE PROFILE

Kenneth D Jordan

University of Pittsburgh

372 PUBLICATIONS **14,108** CITATIONS

SEE PROFILE

Molecular Dynamics Simulations of Methane Hydrate Using Polarizable Force Fields

H. Jiang,[†,‡] K. D. Jordan,*[,†,‡] and C. E. Taylor[‡]

Department of Chemistry and Center for Molecular and Material Simulations, University of Pittsburgh, Pittsburgh, Pennsylvania 15260, and U.S. Department of Energy National Energy Technology Laboratory, Pittsburgh, Pennsylvania 15236

Received: December 11, 2006; In Final Form: February 21, 2007

Molecular dynamics simulations of methane hydrate have been carried out using the polarizable AMOEBA and COS/G2 force fields. Properties calculated include the temperature dependence of the lattice constant, the OC and OO radial distribution functions, and the vibrational spectra. Both the AMOEBA and COS/G2 force fields are found to successfully account for the available experimental data, with overall somewhat better agreement with experiment being found for the AMOEBA model. Comparison is made with previous results obtained using TIP4P and SPC/E effective two-body force fields and the polarizable TIP4P-FQ force field, which allows for in-plane polarization only. Significant differences are found between the properties calculated using the TIP4P-FQ model and those obtained using the other models, indicating an inadequacy of restricting explicit polarization to in-plane only.

I. Introduction

Although the most stable forms of ice have structures in which the water network forms hexagonal "rings", in the presence of small molecules such as methane and at high enough pressures and low enough temperatures, type I clathrates comprised of dodecahedral and tetrakaidecahedral water cages can form, with the guest molecules occupying the cages.[1] Methane hydrate, in particular, has attracted considerable interest due to its formation in natural gas pipelines and the discovery that its deposits on the bottom of ocean floors and in the permafrost contain most of the natural gas on Earth.[2] Not surprisingly, methane hydrate has been the subject of several computer simulations.[3−11] Except for recent simulations[6,8] using the TIP4P-FQ model,[12] all of these simulations employed effective two-body models of the water−water and water−methane interactions. The TIP4P-FQ model allows explicitly for in-plane polarization but not for out-of-plane polarization.[12] In this work, we report the results of molecular dynamics (MD) simulations of methane hydrate using the AMOEBA[13] and COS/G2[14] polarizable water models. As described below, both of these models allow for out-of-plane polarization, with the AMOEBA model employing three polarizable sites and the COS/G2 model a single polarizable site for water. The AMOEBA and COS/G2 models have been shown previously to provide a good description of liquid water as well as of ice Ih.[13,14] Properties of methane hydrate examined include the temperature dependence of the lattice constants, various radial distribution functions, and vibrational spectra.

II. Computational Details

The AMOEBA force field employs distributed multipoles through the quadrupole as well as distributed point polarizable sites on all atoms of the water and methane molecules.[13] In addition, buffered R^{-7} plus R^{-14} interactions are employed between all atoms of different molecules to account for dispersion and short-range repulsion. The AMOEBA model has been found to provide a realistic description of both water clusters and bulk water.[13,15] Due to the computational demands of this model and the fact that it has not been implemented in parallel, its application has been limited to relatively small systems and short simulation times.

The COS/G2 water model, adopts a TIP4P[16]-like rigid backbone, uses three point charges for electrostatics, and employs a mobile point charge attached harmonically to the so-called M-site (see Figure 1) to represent induced polarizability.[14] Short-range repulsion and dispersion interactions between water molecules are accommodated via O−O Lennard−Jones terms. In the simulations using this model, a rigid, nonpolarizable model of methane was adopted. Partial charges were employed on the C and H atoms of methane to represent its electrostatic potential, and a single Lennard−Jones site, located on the C atom was employed to account for repulsion and dispersion interactions. The charges and Lennard−Jones parameters are taken from ref 6. The Lorentz−Berthelot combination rule[17] was used to determine the parameters of Lennard-Jones potentials between the water and methane molecules. Parallel implementations of the COS/G2 model are available in the GROMACS[18,19] and DL_POLY[20] codes.

Since the methane−water interaction potential is a key quantity in the theoretical characterization of methane hydrate, it is important to establish that the model potentials employed provide a reasonable description of this interaction. Figure 2 depicts for the H_2O-CH_4 system potential energy curves calculated using the COS/G2 and rigid-monomer AMOEBA models together with the corresponding curves calculated from ab initio calculations, in particular, using symmetry-adapted perturbation theory (SAPT).[21] The orientation of the monomers used in calculating the potential energy curves is shown in the figure. From this figure it is seen that both the COS/G2 and AMOEBA models give potential energy curves in fairly good agreement with the ab initio curves, with the COS/G2 model giving weaker binding and the AMOEBA model somewhat

* Corresponding author.
† University of Pittsburgh.
‡ NETL.

10.1021/jp068505k CCC: $37.00
Published on Web 05/19/2007

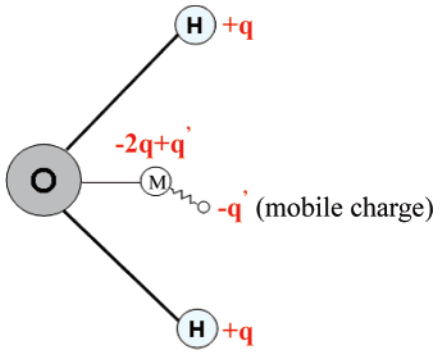

Figure 1. Schematic illustration of the COS/G2 model for water. With the parametrization of ref 14, q and $q' = 0.5265$ and 8.0, respectively, and the M site is located 0.22 Å from the O atom.

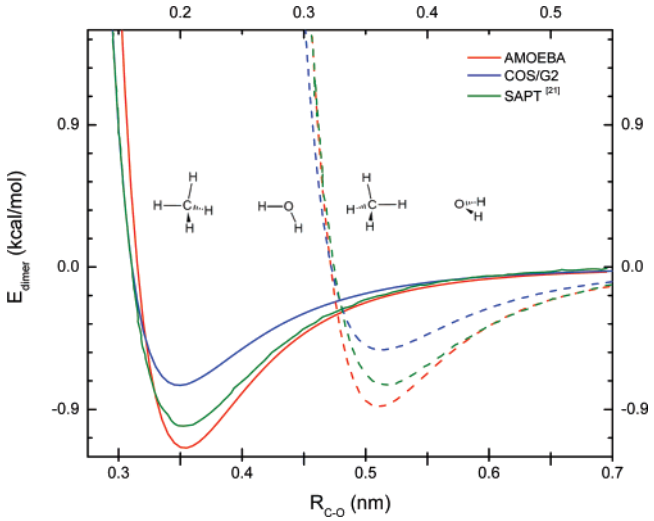

Figure 2. Interaction energy of the methane−water dimer as a function of C−O separation for the two orientations shown in the insets. For easier readability, different horizontal axes are used for the two orientations, with the axis for the orientation on the left side (right side) being on the bottom (top) of the figure. Results are shown for the COS/G2 and AMOEBA models as well as from ab initio SAPT calculations. The SAPT results are from ref 21.

stronger than the SAPT calculations, and with agreement with the ab initio curves being better in the case of the AMOEBA force field.

MD simulations were carried out in both the NVT and NPT ensembles, using a cubic supercell with eight ($2 \times 2 \times 2$) fully occupied unit cells. In the NVT simulations, the box length was taken to be 24.06 Å, consistent with the experimentally determined unit cell length of 12.03 Å for the hydrate of ethylene oxide at $T = -25$ °C.[22] In the starting structure, the positions of the oxygen atoms of the water molecules were taken from the X-ray diffraction structure of the ethylene oxide hydrate,[22] the orientations of the water molecules were initialized in a random fashion according to the Bernal−Fowler rules,[23] and the methane molecules were placed at the centers of the cages.

The intermolecular van der Waals interactions were cut off at a distance of 10.0 Å, with long-range corrections[17] being applied for the energy and pressure. The long-range electrostatics were handled by Ewald summation.[17,24] The NVT and NPT simulations employed the Berendsen weak-coupling thermostat and barostat,[17] respectively, with the corresponding coupling constants being $\tau_T = 0.1$ ps and $\tau_P = 0.5$ ps.

The simulations with the COS/G2 model and most of the simulations with the AMOEBA model were carried out using rigid monomers and time steps of 2 and 4 fs, respectively. In

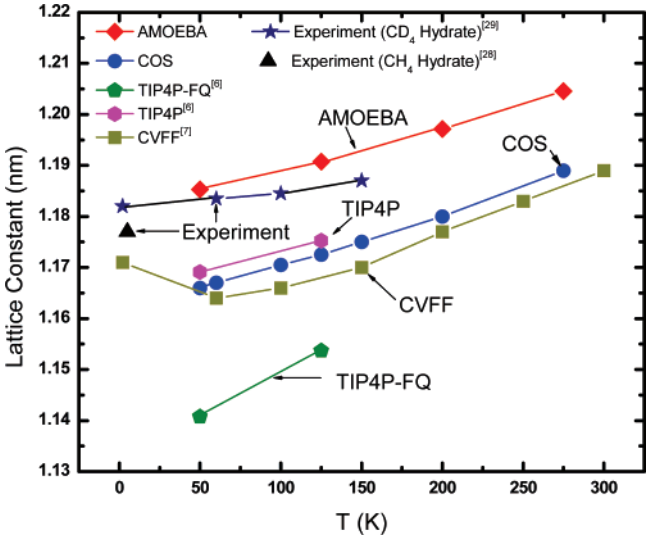

Figure 3. Lattice constant of methane hydrate as a function of temperature. The simulations using the AMOEBA, COS, TIP4P, and TIP4P-FQ models were carried out with $P = 1$ bar. The simulations using the CVFF model were performed at $P = 0$ bar.

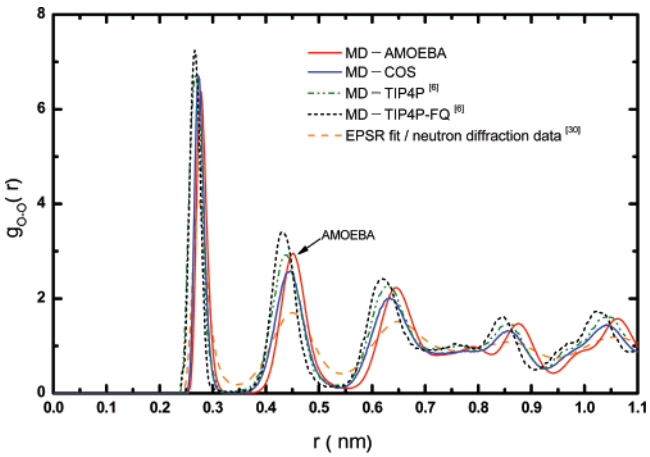

Figure 4. Oxygen−oxygen radial distribution functions. The simulation results are for $T = 200$ K and $P = 20$ bar. The results with the TIP4P and TIP4P-FQ models are from ref 6.

these simulations the bond lengths and bond angles of the monomers were held fixed at their equilibrium values, as defined in the COS/G2 and AMOEBA models, by use of the RATTLE algorithm.[17,25] In addition, for the purpose of calculating the C−H stretch vibrational spectra, simulations were carried out using the AMOEBA model with flexible monomers and a time step of 1 fs. The first 50 ps of each simulation were used for equilibration. The averages were carried out over simulation times of 50 and 450 ps with the AMOEBA and COS/G2 models, respectively. The calculations using the AMOEBA model were carried out using the TINKER[26] code and those using the COS/G2 model were carried out using the GROMACS[18,19] code.

The energy was well conserved in all simulations, indicating that the time steps chosen are adequate. This was also justified by carrying out shorter simulations with smaller time steps (2 fs for AMOEBA/rigid monomers and 0.5 fs for AMOEBA/flexible monomers). The simulations carried out with the shorter time steps gave properties (radial distribution functions and vibrational spectra) nearly identical to those obtained from the simulations carried out with the larger timesteps (except for the poorer statistics due to the shorter production runs).

TABLE 1: Calculated Properties for Methane Hydrate from NVT Simulations Using Various Force Fields

	avg. potential energy (kcal/mol)			avg. dipole moment of water monomers (Debye)			pressure (kbar)		
model	50 K	125 K	200 K	50 K	125 K	200 K	50 K	125 K	200 K
AMEOBA[a]	−11.80	−11.37	−10.91	2.92	2.89	2.86	−3.8	−1.8	0.0
COS/G2[a]	−11.85	−11.42	−10.98	2.82	2.79	2.77	−4.8	−2.4	−0.1
TIP4P−FQ[b]	−12.02	−11.60	−11.15	2.94	2.93	2.90	−14.1	−10.8	−7.6
TIP4P[b]	−11.51	−11.10	−10.66	2.18	2.18	2.18	−8.7	−6.3	−4.1
SPC/E[b]	−12.38	−11.96	−11.52	2.35	2.35	2.35	−9.5	−7.1	−4.8

[a] Present study. [b] From ref 6.

III. Results and Discussions

Properties from NVT Simulations. The average potential energies, molecular dipole moments, and equilibrium pressures from the rigid monomer NVT simulations with the AMOEBA and COS/ G2 models for $T = 50$, 125, and 200 K are reported in Table 1, together with previously reported[6] results obtained for the same conditions with the TIP4P, SPC/E, and TIP4P-FQ models. The simulations with the AMOEBA and COS/G2 models give similar values for the average potential energies, slightly smaller in magnitude than those obtained using the TIP4P-FQ model.[6] On the other hand, the TIP4P model gives appreciably smaller (in magnitude) and the SPC/E model gives appreciably larger (in magnitude) potential energies. The simulations of methane hydrate with the three polarizable models give similar values for the dipole moments for the water monomers, with the average values being about 1 D larger than those of the corresponding gas-phase monomers and several tenths of a Debye larger than those associated with the SPC/E and TIP4P models.

From Table 1 it is also seen that the NVT simulations with the various model potentials give very different values of the pressure. For example, for $T = 200$ K, the simulations with the AMOEBA and COS/G2 models give pressures near 0 kbar, those with the TIP4P and SPC/E models give pressures of −4 to −5 kbar, and those with the TIP4P-FQ model give a pressure of −7.6 kbar. Thus, the simulations with the two effective two-body and the TIP4P-FQ model potentials give pressures that are unphysical, as was noted previously by English and MacElroy.[6] Water models that explicitly allow for both in-plane and out-of-plane polarization give more physically meaningful values for the pressure.

NPT Simulations. The variation of the lattice constant of methane hydrate with temperature was examined by carrying out NPT MD simulations with the AMOEBA and COS/G2 models. Figure 3 reports the resulting lattice constants as well as the values calculated previously using the TIP4P, TIP4P-FQ, and CVFF[27] models,[6,7] together with the experimentally determined lattice constants.[28,29] The CVFF model essentially combines the SPC model for water and an analogous point-charge model for methane with a force field allowing for geometrical relaxation of the monomers.[27] The CVFF results are for a pressure of 0 bar; the other simulations employed a pressure of 1 bar. In comparing the calculated lattice constants with experiment, we focus on the experimental results for CD_4 hydrate rather than for CH_4 hydrate because results are available for a range of temperatures (4.2 − 150 K) for CD_4 hydrate[29] but only for $T = 5.2$ K for CH_4 hydrate.[28]

The simulations with all force fields considered predict that the lattice constant increases in a near linear manner with increasing temperature, in agreement with experiment. (With the CVFF model, the lattice constant has been reported to decrease in going from $T = 0$ to 50 K; however, the $T = 0$ K was obtained by direct geometry optimization rather than from simulations.) Of the model potentials considered, the AMOEBA model gives lattice constants in closest agreement with experiment, with the calculated lattice constants being slightly larger than those measured experimentally. Over the temperature range of $T = 60$ to 300 K, the lattice constants predicted using the COS/G2 model are consistently about 0.15 Å smaller than those calculated using the AMOEBA model and, in fact, are quite close to those obtained previously using the TIP4P and CVFF models.[6,7] The lattice constant from the simulations with the TIP4P-FQ model[6] is appreciably smaller (by 0.03−0.04 Å) than that obtained using the other model potentials considered or obtained experimentally. For all model potentials considered, the calculations predict a greater rate of expansion of the lattice with increasing temperature (from $T \approx 50$ to 150 K) than is found experimentally, with the greatest rate of expansion being predicted with the TIP4P-FQ model. Quantum effects, which are not included in the simulations, may be responsible for the different temperature dependences of the measured and calculated lattice constants (although, in the case of the TIP4P-FQ model, much of the discrepancy between theory and experiment appears to be due to a discrepancy in the model potential).

Radial Distribution Functions. The water−water, methane-water, and the methane−methane radial distribution functions (RDF), $g_{O-O}(r)$, $g_{C-O}(r)$, and $g_{C-C}(r)$, respectively, obtained from the NPT simulations using the AMOEBA and COS/G2 models at $T = 200$ K and $P = 20$ bar are reported in Figures 4−6. These figures also report RDFs from earlier simulations[6] with the TIP4P and TIP4P-FQ models and using the same temperature and pressure as well as RDFs generated by empirical potential structure refinement (EPSR) fits to neutron diffraction data recorded at $T = 279$ K and $P = 145$ bar.[30] (Results are also available for the SPC/E model but are not plotted as they are similar to the TIP4P results.) For all three RDFs, the peaks in the curves generated from the EPSR analysis are lower and broader than those from the MD simulations. In part, this is a consequence of the higher temperature employed in the experimental study (279 K in the experiments vs 200 K in the simulations). However, much of the discrepancy between the simulations and experiment remains even when the simulations are carried out at the same temperature and pressure as used in the experiments. Part of the discrepancy is almost certainly due to the neglect of quantum effects in the simulations, as simulations of both liquid water and ice Ih have shown that the peaks in the O−O RDF are lowered and broadened by inclusion of quantum effects.[31] However, as discussed below, other factors are also at play in the case of the C−O and C−C RDFs.

Of the model potentials considered, the best overall agreement between the calculated and EPSR $g_{O-O}(r)$ is found for the AMOEBA model. In particular, the positions of the first three peaks calculated using the AMOEBA model are in excellent agreement with the EPSR results. The greatest disagreement between the calculated and experimentally deduced peak positions in $g_{O-O}(r)$ is found for the TIP4P-FQ model; with

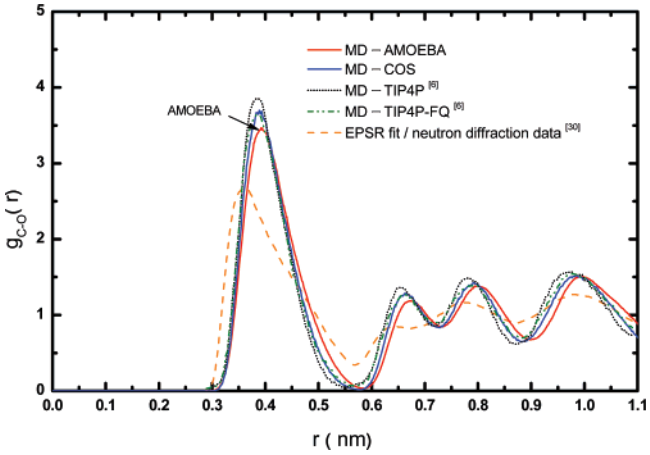

Figure 5. Oxygen−carbon radial distribution functions. The simulation results are for $T = 200$ K and $P = 20$ bar. The results with the TIP4P and TIP4P-FQ models are from ref 6.

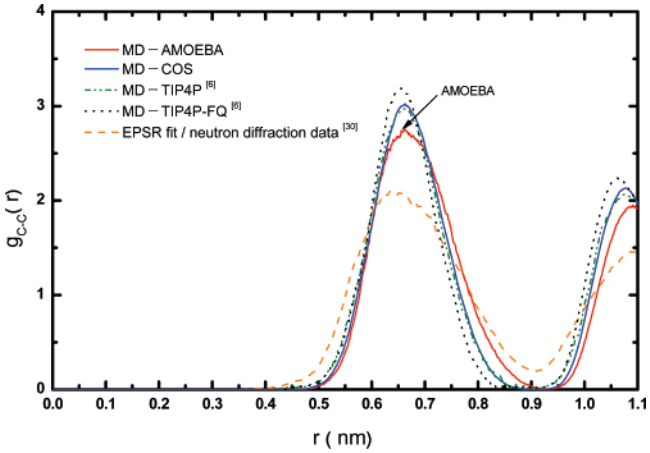

Figure 6. Carbon−carbon radial distribution functions. The simulation results are for $T = 200$ K and $P = 20$ bar. The results with the TIP4P and TIP4P-FQ models are from ref 6.

the COS/G2 and TIP4P models peak positions intermediate between those from the AMOEBA and TIP4P-FQ models are obtained.

The peaks in the EPSR $g_{C-O}(r)$ and $g_{C-C}(r)$ distribution functions are considerably more asymmetrical than those obtained from simulation using any of the model potentials considered. This raises the possibility that much of the discrepancy between the $g_{C-O}(r)$ and $g_{C-C}(r)$ distribution functions from the molecular dynamics simulations and the corresponding distribution functions from the EPSR analysis may be a consequence of assumptions and approximations made in the EPSR procedure for generating the radial distribution functions from the total structure factor, which, in fact, is the quantity measured experimentally.

To test this possibility we have calculated the structure factors for methane hydrate using the SPC/E model and a 60 Å box size, which is more consistent with the experimental measurements than that used in the simulations presented above. (With this box size, the simulations using the polarizable models would have been computationally prohibitive.) The same temperature and pressure ($T = 279$ K, $P = 145$ bar) were used as employed in the neutron diffraction measurements.[30]

Figure 7 compares the total structure factor from the neutron diffraction study of ref 30, that from our MD simulations, and a "hybrid" structure factor generated from the calculated RDFs, but substituting for the C−O RDF that from the EPSR analysis.

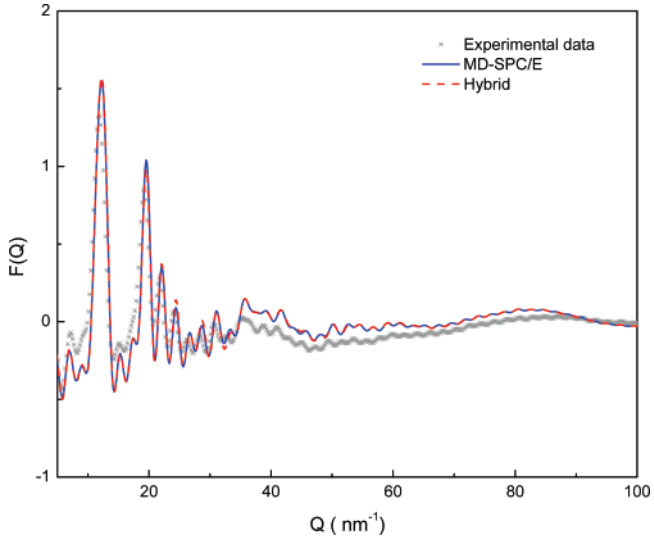

Figure 7. Total structure factor of methane hydrate. The experimental curve is from ref 30 and obtained from neutron diffraction measurements at $T = 279$ K and $P = 145$ bar. The curve labeled MD-SPC/E was obtained from MD simulations at $T = 279$ K and $P = 145$ bar and using the SPC/E model. The "hybrid" structure factor was generated by substituting the C−O RDF from the EPSR analysis of ref 30 for the C−O RDF from the MD simulations.

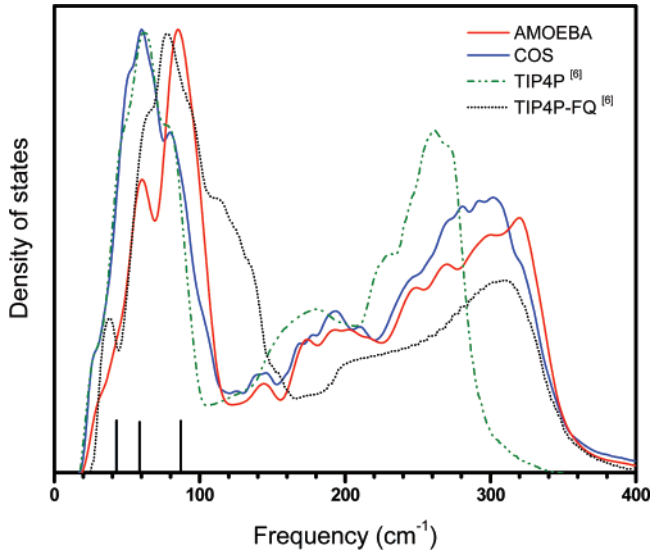

Figure 8. Calculated translational spectra of the host lattice ($T = 200$ K and $P = 20$ bar). The results with the TIP4P and TIP4P-FQ models are from ref 6. The vertical lines indicate the positions of peaks in the experimental INS spectrum (from ref 32).

The structure factor calculated using data from the MD simulation alone is nearly identical to that from the "hybrid" approach and both of these are in fairly good agreement with the experimentally determined structure factor. This is also the case if we substitute the MD results for both the C−O and C−C RDFs in constructing the hybrid factor. This exercise demonstrates that the C−O and C−C distribution functions from the MD simulations are consistent with the experimental structure factor, and more importantly, that the C−O RDFs from the MD simulations and from the EPSR analysis, while appreciably different, are both consistent with the measured structure factor. Thus it appears likely that the high asymmetry in the C−O and C−C RDFs from the EPSR analysis is, in fact, a consequence of assumptions in the EPSR procedure. Further support for this conclusion comes from the observation that the EPSR procedure

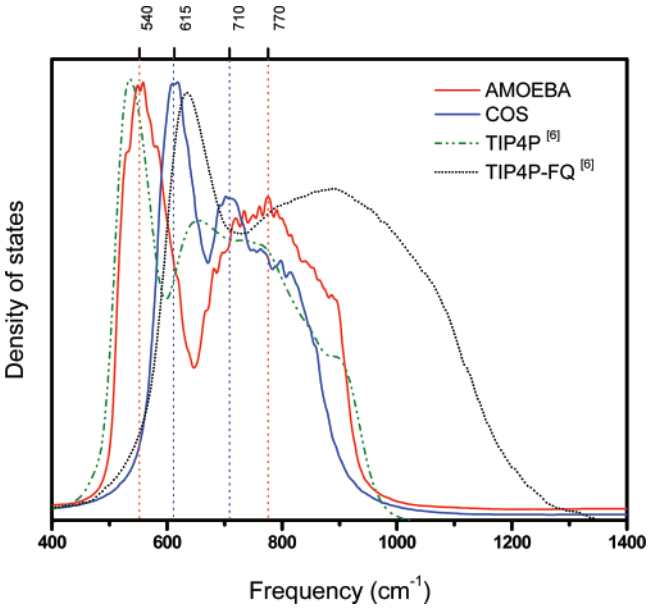

Figure 9. Calculated librational spectra of the host lattice ($T = 200$ K and $P = 20$ bar). The red and blue dashed vertical lines indicate the positions of peaks obtained using the AMOEBA and COS models, respectively. The results with the TIP4P and TIP4P-FQ models are from ref 6.

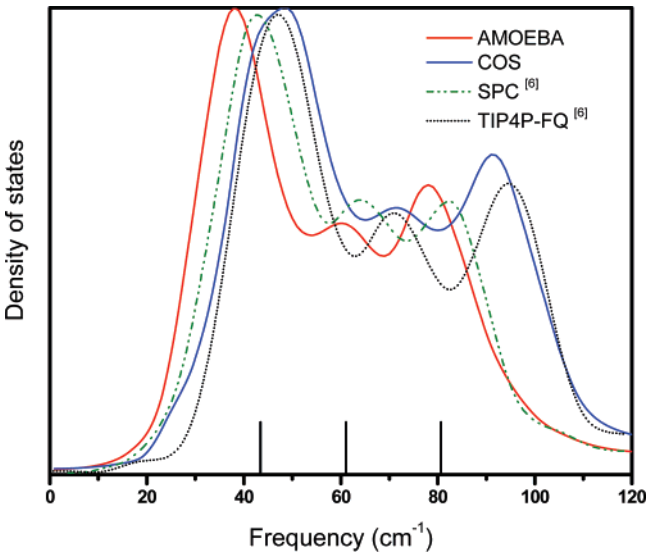

Figure 10. Calculated spectra due to the rattling motion of the encaged methane molecules ($T = 200$ K and $P = 20$ bar). The results with the SPC and TIP4P-FQ models are from ref 6. The vertical lines indicate the positions of peaks in the experimental INS spectrum (from ref 32).

predicts a sizable value for $g_{C-O}(r)$ near $r = 5.7$ Å, where the model potentials predict it to be near zero.

Power Spectra. MacElroy and English have reported power spectra of methane hydrate calculated from the autocorrelation function of the velocities from NPT simulations using the TIP4P, SPC/E, and TIP4P-FQ models, a temperature of 200 K, and a pressure of 20 bar.[6] In the present work, we use the same approach and conditions to obtain the power spectra of methane hydrate using the AMOEBA and COS/G2 model potentials. The low-frequency power spectra associated with the oxygen and hydrogen atoms of the water molecules are depicted in Figure 8 and 9, respectively. These may be associated, respectively, with the density of states of the translational and librational modes of the host lattice. Figure 10 depicts the power spectrum associated with the carbon atoms which is dominated by the rattling motion of the encaged methane molecules. Although the calculated spectra display structure throughout most of the 0 to 3200 cm^{-1} region, experimental vibrational spectra of methane hydrate are available only at very low (<100 cm^{-1}) frequencies as well as in the C−H stretch region.

In discussing the power spectra associated with the water oxygen atoms, we first consider the region below 100 cm^{-1}. All theoretical models considered give three peaks below 100 cm^{-1} due to the transverse acoustic modes of the lattice.[3] The peaks are calculated to occur at 32, 60, and 80 cm^{-1} with the AMOEBA model and at 28, 60, and 85 cm^{-1} with the COS/G2 model. In both cases, the feature near 30 cm^{-1} appears as a weak shoulder. Similar values of the frequencies of the acoustic moles are predicted with the TIP4P and SPC/E nonpolarizable models as well as with the TIP4P-FQ model.[6] The calculated frequencies of the transverse acoustic modes agree reasonably well with the recently reported experimental frequencies (from INS measurements for CD_4 hydrate at $T = 150$ K) of 42.7, 58.9, and 87.9 cm^{-1}.[32] The simulations with the TIP4P, COS/G2, and AMOEBA models produce a pronounced peak near 180 cm^{-1} and a weak peak near 140 cm^{-1} (the latter being more pronounced with the AMOEBA and COS/G2 models than with the TIP4P model) which is due to the longitudinal acoustic modes.[3] With the TIP4P-FQ model the structure due to the longitudinal acoustic modes appears near 120 and 200 cm^{-1}. The simulations with the three polarizable models give a broad peak, due to translational motion of the water molecules, between about 220 and 360 cm^{-1} in the oxygen atom power spectrum. In contrast, with the nonpolarizable SPC/E and TIP4P models, this peak occurs about 70 cm^{-1} lower in frequency.[6]

In ref 6 it was found that the power spectrum associated with the librational motion of the water molecules of methane hydrate is particularly sensitive to the model potential employed. For example, the spectrum calculated using the TIP4P-FQ model differed appreciably from that calculated using the TIP4P and SPC/E models, with the first peak in the spectrum calculated using the TIP4P-FQ potential occurring about 100 cm^{-1} to the blue of the first peak in the spectra from the nonpolarizable models. In addition, with the TIP4P-FQ model, there was a broad feature spanning the frequency range of 740−1300 cm^{-1}, whereas for the nonpolarizable TIP4P and SPC/E models the librational spectra associated with the water molecules dies out near 950 cm^{-1}. This raises the question whether the high frequency ($\sim$950−1300 cm^{-1}) structure in the librational region of the spectrum calculated with the TIP4P-FQ model (but absent in the spectra calculated using the nonpolarizable models) reflects the need to include explicitly electronic polarization or whether it is an artifact of the TIP4P-FQ model. As seen from Figure 9, the spectra obtained with the AMOEBA and COS/G2 models, like those obtained with the SPC/E and TIP4P models, dies off near 950 cm^{-1}. Hence, we conclude that the structure between 950 and 1300 cm^{-1} in the power spectrum calculated with the TIP4P-FQ model is nonphysical, being a consequence of its inclusion of in-plane polarization only.

The librational spectrum generated using the AMOEBA model spans the frequency range of 470−950 cm^{-1} with peaks at 540 and 770 cm^{-1}, whereas that calculated using the COS/G2 model spans the region 490−950 cm^{-1} with peaks at 615 and 710 cm^{-1}. Thus, in this region of the spectrum, different model potentials that account explicitly for polarization give appreciably different spectra. Unfortunately, there are no

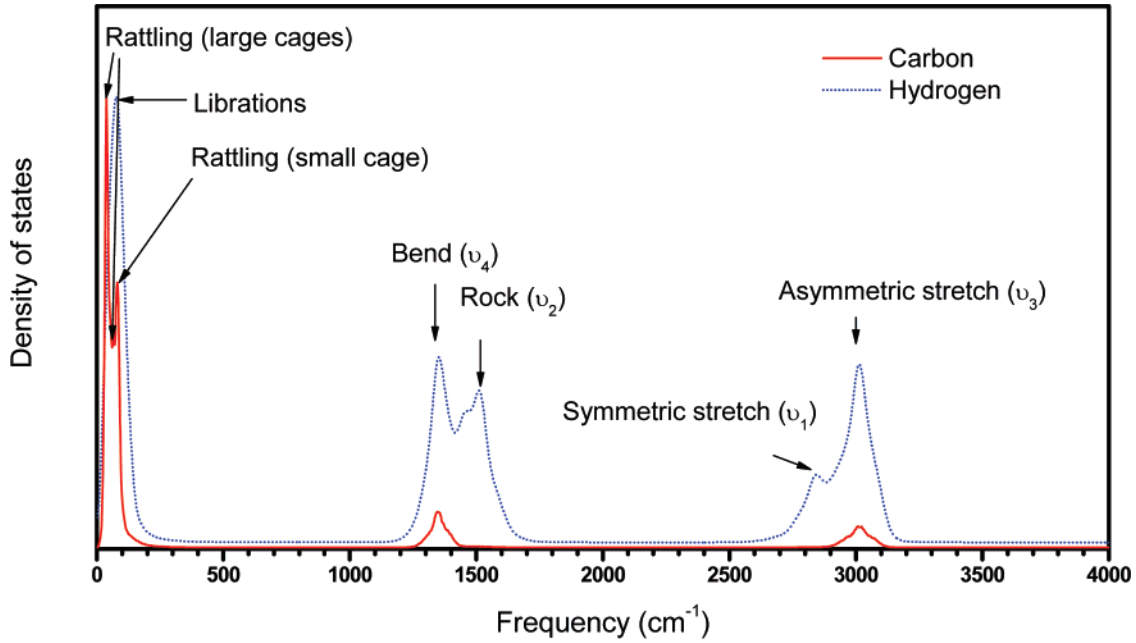

Figure 11. Vibrational spectra of the encaged methane molecules calculated using the AMOEBA model (for $T = 200$ K and $P = 20$ bar).

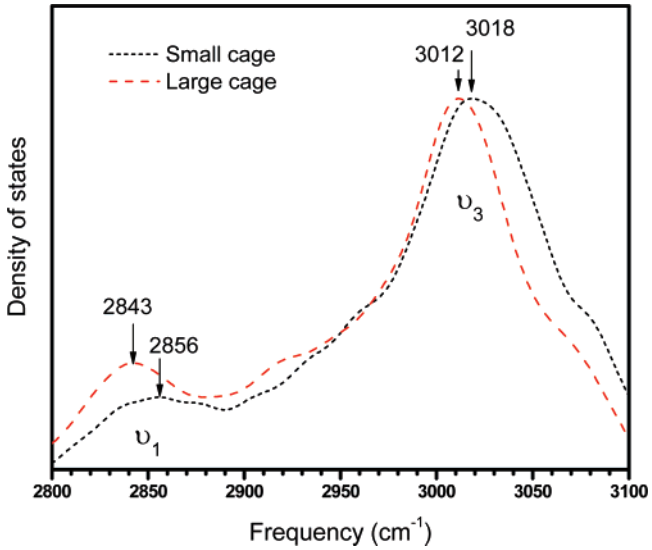

Figure 12. Calculated vibrational spectra associated with the hydrogen atoms of the methane molecules in the small and large water cages ($T = 200$K and $P = 20$ bar).

experimental measurements of the vibrational spectra of methane hydrate in this frequency range.

Figure 10 depicts the power spectra associated with the rattling motion of the methane molecules calculated using AMOEBA, COS/G2, TIP4P-FQ, and SPC force field models. The spectra obtained with the various models are in qualitative agreement, in each case displaying three peaks in the 35−95 cm^{-1} range. The two lower frequency peaks correspond to the translational motion of methane molecules in the large cages, and the high-frequency peak corresponds to the translational motion of methane molecules in the small cages. The peak maxima occur at 38, 60, and 78 cm^{-1} with the AMOEBA model, and at 48, 71, and 91 cm^{-1} with the COS/G2 model. The frequencies of the peak maxima obtained with the TIP4P-FQ model are nearly identical to those from the COS/G2 model. This may be a consequence of the same potential parameters being used for methane in these two models. Overall, the peak positions calculated using the AMOEBA model are in the best agreement with those—43.6, 61.3, and 80.7 cm^{-1}—observed in the experimental $T = 150$ K inelastic neutron scattering (INS) spectrum.[32]

Comparison of Figure 8 and 10 reveals that the peaks due to the translational modes of the water lattice are close to those associated with the translational modes of the methane molecules, consistent with a strong coupling between these degrees of freedom as has been discussed previously in the literature.[33,34] This coupling has been postulated as being responsible for the anomalously low thermal conductivity of methane hydrate.[33,34]

Figure 11 reports the power spectra associated with the C and H atoms of the methane molecules of methane hydrate, calculated using the AMOEBA model with flexible monomers. The bending (υ_4), rocking (υ_2), symmetric C−H stretch (υ_1), and asymmetric C−H stretch (υ_3) modes can be assigned by comparing the spectra associated with the C and H atoms. The peaks at 1352 and 1511 cm^{-1} correspond to the methane bending and rocking modes, respectively, whereas the peaks near 3016 and 2850 cm^{-1} correspond to the asymmetric and symmetric CH stretch modes, respectively.

The calculated C−H stretch spectrum was further decomposed into contributions from methane molecules in the small and large cages. The resulting spectra are depicted in Figure 12. The peaks for the asymmetric C−H stretch vibrations are calculated to be 3012 and 3018 cm^{-1} for the methane molecules in the large and small cages, respectively. The corresponding frequencies for the symmetric C−H stretch vibrations are 2843 and 2856 cm^{-1}. The prediction that the frequencies of the C−H stretch vibrations of the methane molecules in the small cages are more blue-shifted than those in the large cages is also supported by MD simulations using nonpolarizable force fields.[7,35] The calculated splitting of 13 cm^{-1} between the peak positions of the symmetric C−H stretch modes for the small and large cages agrees closely with the results of recent Raman spectroscopic measurements,[36,37] for which the frequencies of the C−H symmetric stretch vibrations in the two cavities are 2904 and 2916 cm^{-1}.

IV. Conclusions

Molecular dynamics simulations of methane hydrate have been carried out using the AMOEBA and COS/G2 polar-

izable force fields. With the AMOEBA model, both the water and methane molecules were described using distributed multipoles and distributed polarizable sites. With the COS/G2 model, atom-centered point-charge descriptions of the electrostatics were employed and only the water molecules were treated as polarizable, using a charge-on-a-spring approach. Overall the MD simulations with the AMOEBA and COS/G2 models fare better at reproducing the available experimental data for methane hydrate than do the simulations with force fields that do not explicitly account for polarization or which include in-plane polarization only, with the agreement with experiment being somewhat better with the AMOEBA model.

The calculations reveal that the vibrational spectrum of methane hydrate in the water librational region is especially sensitive to the details of the force field, with significantly different spectra being obtained with the AMOEBA and COS/G2 polarizable models. Unfortunately, experimental spectra are not available in this frequency range. The calculations also predict that the C−H stretch vibrational frequencies of the methane molecules in the small cages are more blue-shifted than those in the large cages, with the calculated splittings being in close agreement with experiment.

Acknowledgment. This research was carried out with the support of a grant from NETL. K.D.J. acknowledges the support of an ORISE faculty fellowship at NETL. We thank Dr. N. English for helpful discussions, and Drs. C. Koh and A. Soper for sharing with us the data from their neutron diffraction studies, and for valuable discussions. The simulations were carried out on computers housed in the University of Pittsburgh's Center for Molecular and Materials Simulations.

References and Notes

(1) Sloan, E. D. *Clathrate Hydrates of Natural Gases*, 2nd: ed.; Marcel Dekker, Inc.: New York, 1998.
(2) Buffett, B. A. *Annu. Rev. Earth Planet. Sci*. **2000**, *28*, 477.
(3) Tse, J. S.; Klein, M. L.; McDonald, I. R. *J. Phys. Chem*. **1983**, *87*, 4198.
(4) Tse, J. S.; Klein, M. L.; McDonald, I. R. *J. Chem. Phys*. **1984**, *81*, 6146.
(5) Chialvo, A. A.; Houssa, M.; Cummings, P. T. *J. Phys. Chem. B* **2002**, *106*, 442.
(6) English, N. J; MacElroy, J. M. D. *J. Comput. Chem*. **2003**, *24*, 1569.
(7) Greathouse, J. A.; Cygan, R. T. *J. Phys. Chem. B* **2006**, *110*, 6428.
(8) English, N. J.; Johnson, K. J.; Taylor, C. E. *J. Chem. Phys*. **2005**, *123*, 244503.
(9) Anderson, B. J.; Tester, J. W.; Borghi, G. P.; Trout, B. L. *J. Am. Chem. Soc*. **2005**, *127*, 17852.
(10) Chihaia, V.; Adams, S.; Kuhs, W. F. *Chem. Phys*. **2005**, *317*, 208.
(11) Docherty, H.; Galindo, A.; Vega, C.; Sanz, E. *J. Chem. Phys*. **2006**, *125*, 074510.
(12) Rick, S. W.; Stuart, S. J.; Berne, B. J. *J. Chem. Phys*. **1994**, *101*, 6141.
(13) Ren, P.; Ponder, J. W. *J. Phys. Chem. B* **2003**, *107*, 5933.
(14) Yu, H.; van Gunsteren, W. F. *J. Chem. Phys*. **2004**, *121*, 9549.
(15) Ren, P.; Ponder, J. W. *J. Phys. Chem. B* **2004**, *108*, 13427.
(16) Jorgensen, W. L.; Chandrasekhar, J.; Madura, J. D.; Impey, R. W.; Klein, M. L. *J. Chem. Phys*. **1983**, *79*, 926.
(17) Allen, M. P.; Tildesley, D. J. *Computer Simulation of Liquids*; Clarendon Press: Oxford, 1987.
(18) Berendsen, H. J. C.; van der Spoel, D.; van Drunen, R. *Comp. Phys. Commun*. **1995**, *91*, 43.
(19) Lindahl, E.; Hess, B.; van der Spoel, D. *J. Mol. Modeling* **2001**, *7*, 306.
(20) Smith, W.; Forester, T. R. *J. Mol. Graphics* **1996**, *14*, 136.
(21) Akin-Ojo, O.; Szalewicz, K. *J. Chem. Phys*. **2005**, *123*, 1343111.
(22) McMullan, R. K.; Jeffrey, G. A. *J. Chem. Phys*. **1965**, *42*, 2725.
(23) Bernal, J. D.; Fowler, R. H. *J. Chem. Phys*. **1933**, *1*, 515.
(24) Ewald, P. P. *Ann. Phys.* **1921**, *64*, 253.
(25) Andersen, H. C. *J. Comput. Phys.* **1983**, *52*, 24.
(26) Ponder, J. W. *TINKER: Software Tools for Molecular Design*, 4.2 ed.; Washington University School of Medicine: Saint Louis, MO, 2001
(27) Dauber-Osguthorpe, P.; Roberts, V. A.; Osguthorpe, D. J.; Wolff, J.; Genest, M.; Hagler, A. T. *Proteins: Struct., Funct., Genet*. **1988**, *4*, 31.
(28) Davidson, D. W.; Handa, Y. P.; Ratcliffe, C. I.; Tse, J. S.; Powell, B. M. *Nature* **1984**, *311*, 142.
(29) Gutt, G.; Asmussen, B.; Press, W.; Johnson, M. R.; Handa, Y. P.; Tse, J. S. *J. Chem. Phys*. **2000**, *113*, 4713.
(30) Thompson, H.; Soper, A. K.; Buchanancand, P.; Aldiwan, N.; Creek, J. L.; Koh, C. A. *J. Chem. Phys*. **2006**, *124*, 164508.
(31) Hernandez de la Pena, L.; Kusalik, P. G. *J. Chem. Phys*. **2006**, *125*, 0545121.
(32) Baumert, J. Ph.D. Thesis, Christian-Albrechts University, Kiel, Germany, 2003.
(33) Tse, J. S.; Ratcliffe, C. I.; Powell, B. M.; Sears, V. F.; Handa, Y. P. *J. Phys. Chem. A* **1997**, *101*, 4491.
(34) Tse, J. S.; Shpakov, V. P.; Murashov, V. V.; Belosludov, V. R. *J. Chem. Phys*. **1997**, *107*, 9271.
(35) Itoh, H.; Kawamura, K. *Ann. N.Y. Acad. Sci.* **2000**, *912*, 693.
(36) Schicks, J. M.; Erzinger, J.; Ziemann, M. A. *Spectrochim. Acta, Part A* **2005**, *61*, 2399.
(37) Sum, A. K.; Burruss, R. C.; Sloan, E. D. *J. Phys. Chem. B* **1997**, *101*, 7371.